



Exploring the optimal way to produce $Z = 100$ – 106 neutron-rich nuclei

Tian Liang Zhao (赵天亮) ^{1,2} Xiao Jun Bao (包小军),³ and Hong Fei Zhang (张鸿飞) ^{1,2,*}

¹*School of Nuclear Science and Technology, Lanzhou University, 730000 Lanzhou, People's Republic of China*

²*School of Physics, Xi'an Jiaotong University, 710049 Xi'an, People's Republic of China*

³*Department of Physics, Collaborative Innovation Center for Quantum Effects, and Key Laboratory of Low Dimensional Quantum Structures and Quantum Control of Ministry of Education, Hunan Normal University, Changsha 410081, People's Republic of China*



(Received 1 May 2023; accepted 18 July 2023; published 2 August 2023)

The synthesis of neutron-rich heavy and superheavy nuclei is one of the key concerns of nuclear physics. There are only two ways to synthesize nuclei $Z > 92$: fusion evaporation reactions and multinucleon transfer reactions. To theoretically unify the description of fusion evaporation reactions and cross sections of multinucleon transfer reactions, the current model of the dinuclear system is further improved in the present work. The traditional statistical approach of calculating the chance of survival of compound nucleus in fusion evaporation reactions is replaced by using GEMINI++. The results reproduce well the experimental values and trends of the evaporation residue cross sections. Further, the best synthesis of $Z = 100$ – 106 even- Z nuclei is predicted using the improved model. The results show that radioactive projectile nuclei can be applied to fusion evaporation reactions for the synthesis of new neutron-rich nuclei.

DOI: [10.1103/PhysRevC.108.024602](https://doi.org/10.1103/PhysRevC.108.024602)

I. INTRODUCTION

The synthesis of unknown neutron-rich nuclei is a fascinating area of research in nuclear physics [1–5]. The study of these nuclei is important for understanding the properties of nuclear matter and the astrophysical processes that produce them. The significance of this field lies in its contribution to our understanding of the structure and properties of atomic nuclei, as well as its potential applications in various fields such as nuclear energy and medicine. One of the primary methods used to synthesize neutron-rich nuclei is through nuclear reactions that involve the collision of heavy ions. These reactions create highly excited nuclei that can decay into neutron-rich isotopes, which can then be separated and studied.

The discovery of neutron-rich nuclei began with nuclear physics in the early 20th century, including the discovery of fission in the 1930s leading to the development of nuclear reactors and atomic bombs. In the 1950s and 60s, neutron-rich nuclei were created through neutron capture, creating new isotopes. Technological advances allowed for greater precision in creating neutron-rich nuclei in the following decades [6–12]. The discovery of neutron-rich isotopes provided new insights into the properties of these nuclei, while astrophysical observations confirmed the role of the r process in the production of heavy elements. Today, new experiments continue to shed light on neutron-rich nuclei and their role in the universe. Neutron-rich nuclei can be created through fusion, spallation, and fragmentation.

The generation of neutron rich nuclei using multinucleon transfer (MNT) processes is one of the main goals of modern

low-energy heavy ion nuclear physics [1–5]. Multinucleon transfer reactions are complex processes that involve the exchange of several nucleons between two colliding nuclei. Theoretical models have played an important role in understanding the underlying physics of these reactions and predicting their outcomes.

Many methods have been developed to interpret and predict the experimental data of MNT reactions. The current theoretical models can be broadly classified into semiclassical models [13–35] and pure microscopic models [36–44]. The semiclassical models such as the GRAZING model [30,31], the GRAZING-F model [32], the dinuclear system (DNS) model [13–23,26–29], and Langevin-type dynamical equations [33–35] have successfully described the production cross sections of heavy and superheavy nuclei. Among them, the improved DNS model can describe the massive nucleon transfer process between two colliding nuclei from the perspective of multidimensional potential energy surface (PES) diffusion by solving the four-variable master equations [19,20]. The results show that the improved DNS model can well describe the observed production cross sections around the average values. Another important theoretical development in the study of multinucleon transfer reactions is the use of microscopic models. These models are based on the fundamental properties of nucleons and their interactions, and can provide a detailed description of the many-body dynamics of the reaction. Microscopic models have been used to study the effects of nuclear structure and dynamics on transfer probabilities and to predict the formation of new neutron-rich nuclei [36–44].

Overall, theoretical advances in MNT reactions have provided important insights into the underlying physics of these complex processes and have helped to guide experimental studies in this area. Further developments in theoretical

*zhanghongfei@lzu.edu.cn

models and computational techniques are likely to lead to new discoveries in the synthesis of heavy neutron-rich nuclei.

Usually the heavy nuclei synthesized by fusion evaporation (FE) reactions are neutron deficient. In contrast, MNT reactions are considered to be an effective way to synthesize neutron-rich nuclei. With the advancement of technology, radioactive nuclei have been involved in nuclear reactions as projectiles. This makes it possible to synthesize neutron-rich nuclei by fusion evaporation reactions. The purpose of this paper is to explore the optimal method of neutron-rich nucleus synthesis at $Z = 100\text{--}106$ and the corresponding combination of projectile targets based on the dinuclear system model.

II. THEORETICAL FRAMEWORK

The DNS model is a theoretical framework used to describe the dynamics of nuclear reactions involving two heavy ions. In this model, the two nuclei are treated as independent clusters that interact through a short-range potential. The potential between the two clusters is assumed to be weak enough that the two nuclei can retain their identities, but strong enough to allow for the exchange of nucleons and the formation of a compound nucleus. The DNS model has been used to explain a variety of nuclear phenomena, including fusion hindrance, the fusion of neutron-rich nuclei, and the decay of highly excited nuclei. It is a powerful tool for understanding the behavior of heavy-ion reactions and for guiding experimental studies of nuclear structure and dynamics.

The cross section that produces a nucleus with proton number Z_1^f and neutron number N_1^f in a heavy ion collision can be

written as [26,27]

$$\begin{aligned} \sigma_{Z_1^f, N_1^f}(E_{c.m.}) &= \frac{\pi \hbar^2}{2\mu E_{c.m.}} \sum_J (2J+1) T(E_{c.m.}, J) \\ &\times \sum_{\beta_1} \sum_{\beta_2} P(Z_1, N_1, \beta_1, \beta_2, J, \tau_{\text{int}}) \\ &\times W(Z_1, N_1; Z_1', N_1', J'), \end{aligned} \quad (1)$$

where $E_{c.m.}$ is the incident energy in the center-of-mass coordinate system, and the transmission probability is

$$\begin{aligned} T(E_{c.m.}, J) &= \int f(B) \frac{1}{1 + \exp\left\{-\frac{2\pi}{\hbar\omega(J)} [E_{c.m.} - B - \frac{\hbar^2}{2\mu R_B^2} J(J+1)]\right\}} dB. \end{aligned} \quad (2)$$

The detailed derivation procedure and parameters can be obtained from Ref. [45]. The range of angular momentum J is from zero to grazing angular momentum. If the incident energy is higher than the Coulomb barrier, the penetration coefficient $T(E_{c.m.}, J)$ in Eq. (1) is estimated to be 1.

In heavy-ion collisions near the Coulomb barrier, the nucleon transfer processes can be described as a diffusion process by numerically solving a set of four-variable master equations (MEs). The evolution of the probability distribution function $P(Z_1, N_1, \beta_1, \beta_2, t)$ in Eq. (1) can be expressed by [26,27]

$$\begin{aligned} \frac{dP(Z_1, N_1, \beta_1, \beta_2, t)}{dt} &= \sum_{Z_1'} W_{Z_1, N_1, \beta_1, \beta_2; Z_1', N_1, \beta_1, \beta_2}(t) [d_{Z_1, N_1, \beta_1, \beta_2} P(Z_1', N_1, \beta_1, \beta_2, t) - d_{Z_1', N_1, \beta_1, \beta_2} P(Z_1, N_1, \beta_1, \beta_2, t)] \\ &+ \sum_{N_1'} W_{Z_1, N_1, \beta_1, \beta_2; Z_1, N_1', \beta_1, \beta_2}(t) [d_{Z_1, N_1, \beta_1, \beta_2} P(Z_1, N_1', \beta_1, \beta_2, t) - d_{Z_1, N_1', \beta_1, \beta_2} P(Z_1, N_1, \beta_1, \beta_2, t)] \\ &+ \sum_{\beta_1'} W_{N_1, Z_1, \beta_1, \beta_2; N_1, Z_1, \beta_1', \beta_2}(t) [d_{Z_1, N_1, \beta_1, \beta_2} P(Z_1, N_1, \beta_1', \beta_2, t) - d_{Z_1, N_1, \beta_1', \beta_2} P(Z_1, N_1, \beta_1, \beta_2, t)] \\ &+ \sum_{\beta_2'} W_{N_1, Z_1, \beta_1, \beta_2; N_1, Z_1, \beta_1, \beta_2'}(t) [d_{Z_1, N_1, \beta_1, \beta_2} P(Z_1, N_1, \beta_1, \beta_2', t) - d_{Z_1, N_1, \beta_1, \beta_2'} P(Z_1, N_1, \beta_1, \beta_2, t)]. \end{aligned} \quad (3)$$

β_1 and β_2 are considered as two discrete variables [19,20]. They denote quadrupole deformations of the projectilelike fragments (PLFs) and targetlike fragments (TLFs), respectively. $W_{Z_1, N_1, \beta_1, \beta_2; Z_1', N_1, \beta_1, \beta_2}$ is the mean transition probability from channel $(Z_1', N_1, \beta_1, \beta_2)$ to $(Z_1, N_1, \beta_1, \beta_2)$. $d_{N_1, Z_1, \beta_1, \beta_2}$ denotes microscopic dimensions corresponding to the macroscopic state $(N_1, Z_1, \beta_1, \beta_2)$. The transition probabilities are related to the local excitation energy and nucleon transfer by microscopic derivation of the interaction potential in valence space. The proton transition probability can be written as

$$W_{Z_1, N_1, \beta_1, \beta_2; Z_1', N_1, \beta_1, \beta_2} = \frac{\tau_{\text{mem}}(Z_1, N_1, \beta_1, \beta_2; Z_1', N_1, \beta_1, \beta_2)}{\hbar^2 d_{Z_1, N_1, \beta_1, \beta_2} d_{Z_1', N_1, \beta_1, \beta_2}} \sum_{i, i'} |\langle Z_1', N_1, \beta_1, \beta_2, i' | V(t) | Z_1, N_1, \beta_1, \beta_2, i \rangle|^2, \quad (4)$$

where i denotes all remaining quantum numbers and τ_{mem} is the memory time. The local excitation energy ε^* is defined as

$$\begin{aligned} \varepsilon^*(J) &= E_x(J, t) - [U(N_1, Z_1, N_2, Z_2, R_{\text{cont}}, \beta_1, \beta_2, J) \\ &- U(N_P, Z_P, N_T, Z_T, R_{\text{cont}}, \beta_{10}, \beta_{20}, J)], \end{aligned} \quad (5)$$

Detailed descriptions can be found in Refs. [19–21].

The PES of the multinucleon rearrangement in the DNS model is defined as [26]

$$\begin{aligned} U(N_1, Z_1, N_2, Z_2, R_{\text{cont}}, \beta_1, \beta_2, J) \\ = B_{\text{mac}}(N_1, Z_1, \beta_1) + B_{\text{mic}}(N_1, Z_1, \beta_1) \end{aligned}$$

$$\begin{aligned}
& + B_{\text{mac}}(N_2, Z_2, \beta_2) + B_{\text{mic}}(N_2, Z_2, \beta_2) \\
& + V_{CN}(N_1, Z_1, N_2, Z_2, R_{\text{cont}}, \beta_1, \beta_2) \\
& + V_{\text{rot}}(N_1, Z_1, N_2, Z_2, R_{\text{cont}}, \beta_1, \beta_2, J), \quad (6)
\end{aligned}$$

where $N = N_1 + N_2$ and $Z = Z_1 + Z_2$, and β_1 and β_2 represent quadrupole deformations of the PLF and TLF, respectively. The binding energy and deformation are derived from the improved macroscopic microscopic model [46].

The nucleon transfer process is assumed to occur at $R_{\text{cont}} = R_1[1 + \beta_1 Y_{20}(\theta_1)] + R_2[1 + \beta_2 Y_{20}(\theta_2)] + 0.5$ fm, with $R_i = 1.16A_i^{1/3}$. The deformation dependent binding energies $B(N_1, Z_1, \beta_1)$ and $B(N_2, Z_2, \beta_2)$ are calculated by macroscopic-microscopic models. These will be specified in the next subsection. The nucleus-nucleus interaction potential energy V_{CN} between two interacting nuclei of the DNS configuration is the sum of the nuclear interaction potential V_N obtained from the folding integral of a zero-range nucleon-nucleon interaction [47,48] and Coulomb interaction potential V_C calculated by Wong's formula [49]. The rotational energy $V_{\text{rot}} = \hbar^2 J(J+1)/I_{\text{tot}}$, where the moment of inertia I_{tot} is approximated by its rigid-body value.

When the primary product is produced, the deformation of PLF nucleus and TLF nucleus in the exit channel is no longer the ground state deformation, and the excitation energy of the primary fragment nucleus is expressed as

$$E_{\text{tot}} = E_{\text{c.m.}} - \text{TKE} + Q_{\text{gg}}. \quad (7)$$

Q_{gg} denotes the energy released during the reaction. Here it is assumed that the excitation energy assigned to the PLF and the TLF is proportional to their masses:

$$E_{Z_1, N_1}^* = E_{\text{tot}} \times \frac{A_1 + A_2}{A_1}, \quad (8)$$

where E_{Z_1, N_1}^* is the excitation energy and A_1 and A_2 are the mass numbers of the corresponding nuclei.

The deexcitation process of this work is simulated using the statistical model GEMINI++ and the default parameters of this model are used for the calculations [50,51]. Subsequent deexcitation cascades of the excited fragments via emission of light particles (neutron, proton, and α) and γ rays competing with the fission process are taken into account, which lead to the final mass distribution of the reaction products. GEMINI++ can be used to describe the deexcitation probability from the primary to the final section of the MNT reaction [26,27,52]. In order to uniformly describe the MNT reaction and fusion evaporation reaction, we also use GEMINI++ to calculate the survival probability of compound nucleus. For a certain primary product, the statistical nature of GEMINI++ requires multiple simulations of its deexcitation process. For the MNT reaction, this paper sets $M_{\text{trial}} = 1000$, and for the FE reaction, $M_{\text{trial}} = 1\,000\,000$ due to the low survival chance of superheavy compound nucleus. After Monte Carlo simulation, the decay probability of the calculated primary product (compound nucleus) to the final product can be estimated as $W(Z_1, N_1; Z'_1, N'_1, J')$. The reliability of the results is verified in the next section.

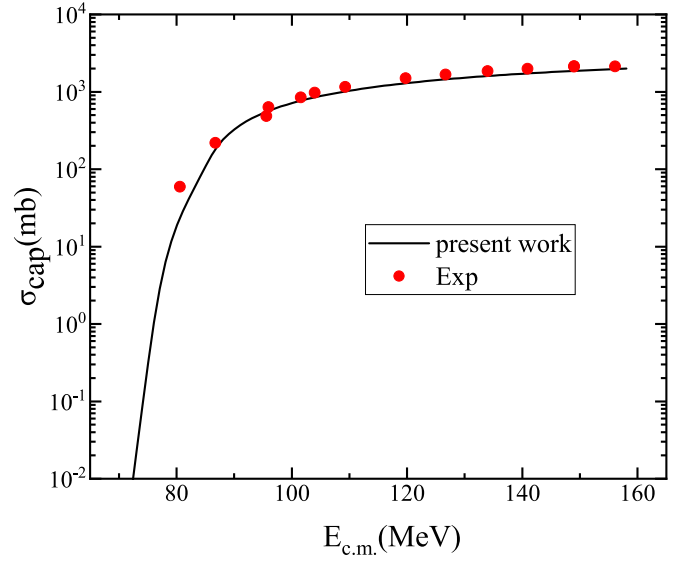


FIG. 1. Comparison of theoretically calculated $^{16}\text{O} + ^{238}\text{U}$ capture cross section with experimental values. The solid black line is the model calculation result and the red circle is the experimental value.

III. RESULTS AND DISCUSSION

A. Validating the DNS model calculation results

To explore optimal synthesis methods for producing $Z = 100$ – 106 neutron-rich nuclei based on a unified approach, it is necessary to first verify the reliability of the previously proposed improved DNS model plus GEMINI++ for calculating the evaporation residue cross section (ERCS). Since the capture cross section is experimentally measurable, we first verified the calculated capture cross section results. We calculated the capture cross section for $^{16}\text{O} + ^{238}\text{U}$ [53], as shown in Fig. 1. The theoretical results reproduced the experimental values very well, indicating that the theoretical model used for calculating the capture cross section is reliable.

In the utmost mass-asymmetric fusion reactions (with lighter than neon projectiles), the formation of composite nuclei is hardly suppressed. The probability of formation of compound nuclei after contact of colliding nuclei is almost 1. This greatly increases the evaporation residue cross section for such reactions, and, although it is rather difficult to produce radioactive nuclei with significant neutron excess, they can be used to study neutron-rich fermium nuclei. In this paper, we approximate the P_{CN} of the fusion evaporation reaction as 1. The P of the MNT reaction is still obtained from the master equation.

Since the value of the probability of survival cannot be directly measured. Next, we use the results of the total cross-section to verify whether the calculation of the survival probability is reasonable. According to the description in Sec. II, we calculated the ERCS for $^{18}\text{O} + ^{248}\text{Cm}$ [54] using the improved DNS model plus GEMINI++ and compared it with the experimental values. The results are presented in Fig. 2. To demonstrate the reliability of using GEMINI++ for calculating the chance of survival of compound nuclei, we

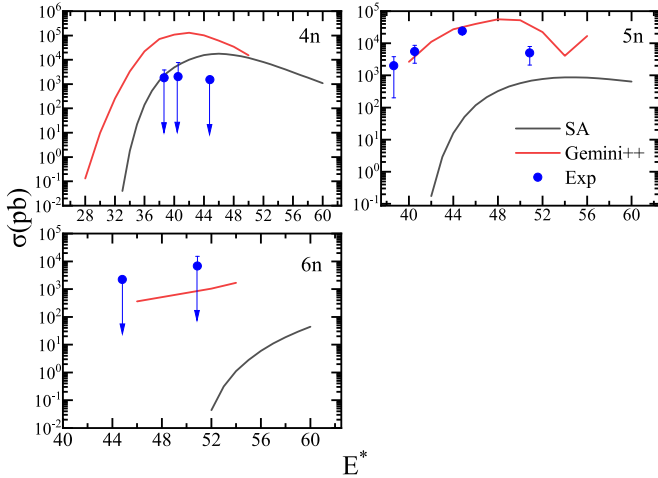


FIG. 2. Theoretical and experimental values of the evaporation residue cross section for the $4n$ - $6n$ channel fusion evaporation reaction $^{18}\text{O} + ^{248}\text{Cm}$. The blue circles indicate the experimental values from Ref. [54], the red solid line indicates the evaporation residue cross section obtained using GEMINI++ to calculate the chance of survival of the compound nucleus, and the black solid line indicates the results using the statistical approach (SA).

also employed a statistical approach (SA) similar to that in Ref. [55] to calculate the survival probability of the compound nucleus and obtain the corresponding evaporation residue cross section. The ERCS values calculated by both methods are shown in Fig. 2.

As we can see in Fig. 2, the results using the statistical method reproduce the results of the $4n$ channels very well, while the results for the $5n$ and $6n$ channel differ significantly from the experimental values. The trend of the evaporation residue cross section cannot be reproduced well. This statistical method has a large uncertainty, which is where we need to improve. In contrast, using GEMINI++ to calculate the survival probability can better reproduce the experimental results of the evaporation residue cross section. The trends of the $4n$, $5n$, and $6n$ channels are well reproduced. This also shows the higher reliability of the GEMINI++ method.

For further validation, we also calculated the evaporation residue cross section for the $5n$ channel of $^{22}\text{Ne} + ^{244}\text{Pu}$ [56]. In Fig. 3 we can see that the evaporation residue cross section obtained using GEMINI++ to calculate the survival probability fits the experimental results better than using the statistical approach. Therefore, we believe that using the GEMINI++ method to calculate the survival chance is more reliable.

The reliability of calculating multinucleon transfer reaction cross sections using the improved DNS model plus GEMINI++ has been verified in many references [26–29]. Here, the actinide target combination $^{238}\text{U} + ^{248}\text{Cm}$ is chosen, with an energy of $E_{c.m.} = 898.71$ MeV under the center-of-mass system. The primary isotopic distributions and the final fragmentation cross section for the target nucleus getting 1–5 protons is depicted in Fig. 4. As we can see in Fig. 4, the improved DNS model reproduces the cross section of the final product well. The cross section of the final fragment is 1–5

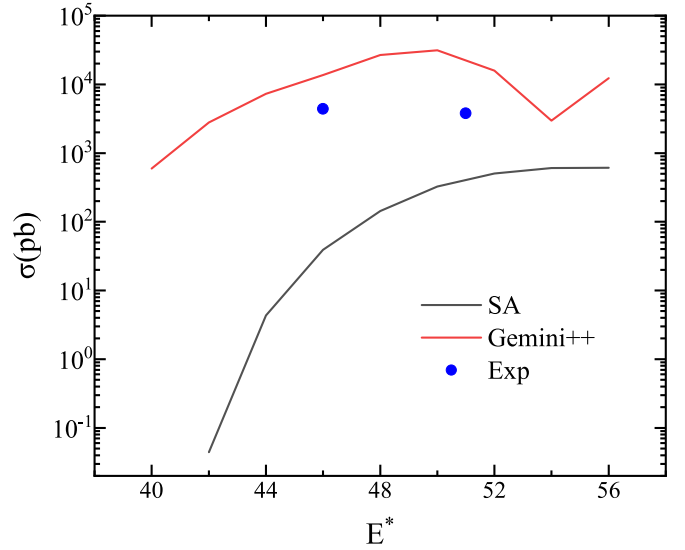


FIG. 3. Theoretical and experimental values of the evaporation residue cross section for the $5n$ channel fusion evaporation reaction $^{22}\text{Ne} + ^{244}\text{Pu}$. The blue circles indicate the experimental values from Ref. [56], the red solid line indicates the evaporation residue cross section obtained using GEMINI++ to calculate the chance of survival of the compound nucleus, and the black solid line indicates the results using the statistical approach (SA).

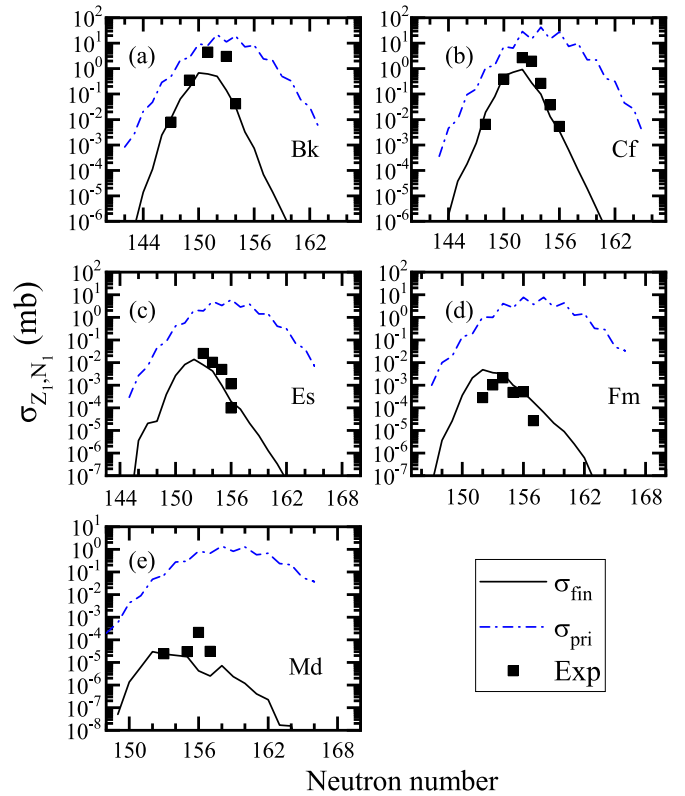


FIG. 4. Comparison of theoretically calculated $^{238}\text{U} + ^{248}\text{Cm}$ at $E_{c.m.} = 898.71$ MeV [7] primary fragments cross section, final fragments cross section, and experimental values. The blue dotted line is the primary fragment cross section, the black solid line is the final fragment cross section, and the black square is the experimental value.

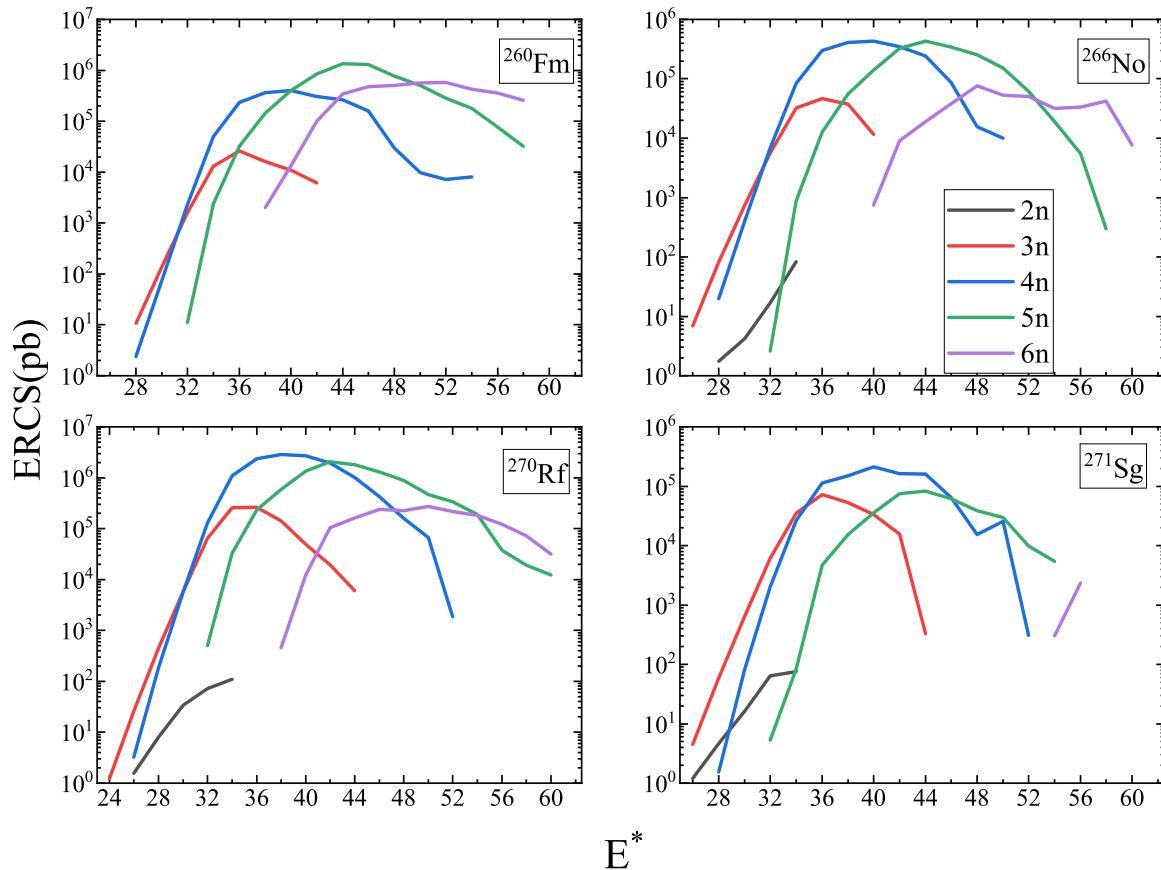


FIG. 5. Theoretical calculation of the evaporation residue cross sections of $^{22}\text{O} + ^{238}\text{U}$, ^{244}Pu , ^{248}Cm , and ^{249}Cf . The black, red, blue, green, and purple solid lines indicate the $2n$ - $6n$ evaporation channels, respectively. The box in the upper right corner is the compound nucleus.

orders of magnitude lower compared to the cross section of the primary fragment. During the survival process, the primary fragments with certain excitation energy may not only evaporate neutrons but also charged particles, or undergo fission. Similarly to compound nuclei in fusion evaporation reactions, heavier excited fragment nuclei can hardly be deexcited by evaporation of only a few neutrons. Therefore, the chances of survival of primary fragment nuclei being deexcited to isotopic final fragment nuclei are low. We also tried to reduce the number of simulations and found that a minimum of 10^6 are needed to get more data with better results in the region close to the superheavy nucleus. For superheavy nuclei with $Z > 110$, more simulations may be required. This will be further investigated in future work. Based on the above discussion, we use the improved DNS model plus GEMINI++ to reproduce well the evaporation residue cross section of the fusion evaporation reaction and the cross section of the MNT reaction. Next, we will predict the best synthesis of neutron-rich nuclei with $Z = 100$ – 106 .

B. $Z = 100$ – 106 neutron-rich nucleosynthesis cross section predictions

The conventionally used stable projectile nuclei and target nuclei are not sufficient for the synthesis of neutron-rich heavy and superheavy nuclei due to the shift of the β stable line. With the advancement of experimental technology, the

use of radioactive projectile nuclei can be considered as a way to synthesize neutron-rich heavy and superheavy nuclei. Based on the previous discussion, we selected ^{22}O as the projectile nucleus. The beam intensity of ^{22}O at the level of 10^8 pps is sufficient to detect one decay event per week [57]. The actinide target nuclei are ^{238}U , ^{244}Pu , ^{248}Cm , and ^{249}Cf . The calculated results of the evaporation residue cross section are plotted in Fig. 5. From Fig. 5 we can see that the $5n$ evaporation channel of the composite core ^{260}Fm has the largest cross section. The remaining three compound nuclei ^{266}No , ^{270}Rf , and ^{271}Sg have the largest cross sections appearing in the $4n$ evaporation channel.

From Fig. 5 we can also see that the results for the evaporation residue cross section have abrupt variations at different energies. This is probably due to the insufficient number of simulations in GEMINI++. If the number of simulations is increased, the curve will be smoother and contain more ERCS corresponding to the excitation energy, but this will significantly increase the calculation time. Our goal is to obtain the best combination of the synthetic neutron-rich nuclei with the corresponding excitation energies. Therefore, the current set of simulations is sufficient for the current calculation.

MNT reactions are also an efficient way to synthesize neutron-rich nuclei. In order to investigate the best way to synthesize neutron-rich heavy and superheavy nuclei. Also based on the improved DNS model plus GEMINI++, we have calculated the transfer reaction cross section for the $^{238}\text{U} + ^{248}\text{Cm}$

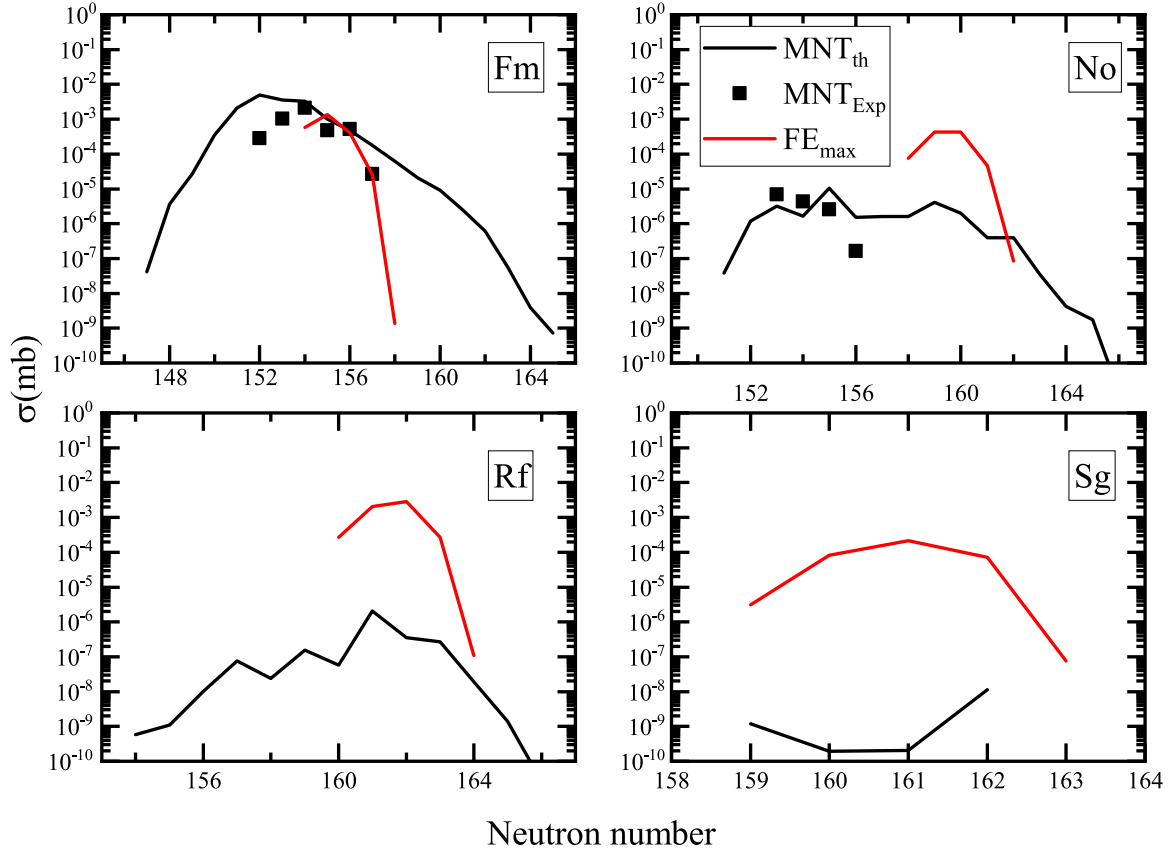


FIG. 6. The cross section of the multinucleon transfer reaction of $^{238}\text{U} + ^{248}\text{Cm}$ at $E_{c.m.} = 898.71$ MeV [7] and the highest cross section of the fusion evaporation reaction corresponding to the target nucleus in Fig. 5. The solid black line is the theoretical value of the multinucleon transfer reaction, the black square is the experimental value of the multinucleon transfer reaction, and the red line is the theoretical value corresponding to the fusion evaporation reaction. The theoretical results are given by the improved DNS model plus GEMINI++.

reaction at $E_{c.m.} = 898.71$ MeV. In Fig. 6, the black solid lines are the theoretical values of the transfer reaction cross sections for the different isotopes of the four elements Fm, No, Rf, and Sg. The black squares indicate the experimental values of the cross sections for the MNT reactions. The red circles indicate the maximum values of the evaporation residue cross sections for the corresponding nuclide under the fusion evaporation reaction of Fig. 5. It can be seen that the improved DNS model plus GEMINI++ reproduces the cross section of the MNT reaction very well.

We can also see from Fig. 6 that the fermium element's abundant neutron isotope has a higher reaction cross section in the MNT reaction, and, with the increase of proton number, the cross section of the MNT reaction decreases rapidly. The cross sections of fusion evaporation reactions with ^{22}O as the nucleus of the projectile do not differ much in size. Except for Fm, the maximum cross sections of the $2n$ evaporation channels of No, Rf, and Sg are around 10^{-7} mb, which is close to the cross section of the MNT reaction. The maximum cross sections of the $3n$ - $6n$ evaporation channels are all significantly higher than the cross sections of the MNT reactions.

Since the MNT reaction cross section decreases rapidly with the number of transferred protons, the greatest difficulty in synthesizing neutron-rich superheavy nuclei lies in the absence of suitable target nuclei. The MNT reaction cross

sections for the heavy actinide nucleus $^{248}\text{Cm} + ^{249}\text{Cf}$ at different energies were calculated in Ref. [26]. A comparison with the cross sections for the fusion evaporation reaction using ^{22}O in present paper still leaves a large gap. Based on the results in this paper, we suggest that the fusion evaporation reaction has a greater possibility of synthesizing neutron-rich isotopes of the three elements No, Rf, and Sg. For each nuclide, the corresponding maximum cross sections for the fusion evaporation reaction are listed in Table I. At the same time, we should acknowledge that the excitation function for the production of a given isotope of transfermium isotopes in the transfer reaction is much wider compared to the fusion excitation functions.

TABLE I. The maximum cross sections achievable for synthesizing the corresponding nuclide via a fusion evaporation reaction.

nuclide	^{260}No	^{261}No	^{262}No	^{263}No
σ (pb)	76443.9	431075	431121	46113.7
nuclide	^{264}Rf	^{265}Rf	^{266}Rf	^{267}Rf
σ (pb)	270816	2049910	2841660	264218
nuclide	^{265}Sg	^{266}Sg	^{267}Sg	^{268}Sg
σ (pb)	3117.75	82478.5	212224	72319.4
				75.4554

IV. CONCLUSIONS

In this paper, the survival chance calculation method in the DNS model is improved. The survival odds in the fusion evaporation reaction were calculated using GEMINI++ instead of statistical methods. A unified description of the evaporation residue cross section and the multinucleon transfer reaction cross section is achieved. The improved DNS model plus GEMINI++ reproduces well the evaporation residue cross section and capture cross section of the oxygen atomic nucleus and the actinide target nucleus. The MNT reaction cross section of the actinide projectile-target combination is also well described. Based on these discussions, the optimal synthesis of $Z = 100$ – 106 even- Z neutron-rich nuclei was predicted. The reaction using the radioactive projectile nucleus ^{22}O and the actinide target nucleus allows the synthesis of neutron-rich isotopes of No, Rf, and Sg. The role of radioactive projectile nuclei is not negligible in the synthesis of neutron-rich superheavy nuclei. This facilitates the experimental synthesis of nuclei near the magic number $N = 162$ and the further investigation of their properties. Further, the structural information of these neutron-rich nuclides can be studied. New insights

into the decay modes and reaction mechanisms of actinide heavy neutron-rich nuclei and superheavy neutron-rich nuclei are provided.

The transfer cross section between the projectile nucleus and target nucleus decreases as the number of nucleons transferred increases. The difficulty of synthesizing neutron-rich superheavy nuclei by MNT reactions is obvious. However, the MNT reaction has considerable advantages in the synthesis of neutron-rich nuclei with $Z \leq 100$. Based on the discussion in this paper, it may be possible to use neutron-rich radioactive projectile nuclei for FE reactions to reach the superheavy stable island. This will be discussed in future work.

ACKNOWLEDGMENTS

X.J.B. is supported by the National Natural Science Foundation of China (Grants No. 12175064 and No. U2167203) and the Hunan Outstanding Youth Science Foundation (Grant No. 2022JJ10031). H.F.Z. is supported by the National Natural Science Foundation of China (Grants No. 12175170 and No. 11675066).

-
- [1] H. Freiesleben and J. V. Kratz, *Phys. Rep.* **106**, 1 (1984).
 [2] J. V. Kratz, W. Loveland, and K. J. Moody, *Nucl. Phys. A* **944**, 117 (2015).
 [3] L. Corradi, G. Pollarolo, and S. Szilner, *J. Phys. G: Nucl. Part. Phys.* **36**, 113101 (2009).
 [4] F. S. Zhang, C. Li, L. Zhu, and P. W. Wen, *Front. Phys.* **13**, 132113 (2018).
 [5] W. D. Loveland, *Front. Phys.* **7**, 23 (2019).
 [6] M. Schädel, J. V. Kratz, H. Ahrens, W. Bröchle, G. Franz, H. Gäggeler, I. Warnecke, G. Wirth, G. Herrmann, N. Trautmann, and M. Weis, *Phys. Rev. Lett.* **41**, 469 (1978).
 [7] M. Schädel, W. Bröchle, H. Gäggeler, J. V. Kratz, K. Sümmerer, G. Wirth, G. Herrmann, R. Stakemann, G. Tittel, N. Trautmann *et al.*, *Phys. Rev. Lett.* **48**, 852 (1982).
 [8] A. G. Artukh, V. V. Avdeichikov, G. F. Gridnev *et al.*, *Nucl. Phys. A* **176**, 284 (1971).
 [9] D. Lee, K. J. Moody, M. J. Nurmi, G. T. Seaborg, H. R. von Gunten, and D. C. Hoffman, *Phys. Rev. C* **27**, 2656 (1983).
 [10] D. C. Hoffman, M. M. Fowler, W. R. Daniels, H. R. von Gunten, D. Lee, K. J. Moody, K. Gregorich, R. Welch, G. T. Seaborg, W. Bröchle *et al.*, *Phys. Rev. C* **31**, 1763 (1985).
 [11] K. J. Moody, D. Lee, R. B. Welch, K. E. Gregorich, G. T. Seaborg, R. W. Lougheed, and E. K. Hulet, *Phys. Rev. C* **33**, 1315 (1986).
 [12] A. Türler, H. R. von Gunten, J. D. Leyba, D. C. Hoffman, D. M. Lee, K. E. Gregorich, D. A. Bennett, R. M. Chasteler, C. M. Gannett, H. L. Hall *et al.*, *Phys. Rev. C* **46**, 1364 (1992).
 [13] G. G. Adamian, N. V. Antonenko, A. Diaz-Torres, and S. Heinz, *Eur. Phys. J. A* **56**, 47 (2020).
 [14] G. G. Adamian, N. V. Antonenko, V. V. Sargsyan, and W. Scheid, *Phys. Rev. C* **81**, 024604 (2010).
 [15] G. G. Adamian, N. V. Antonenko, V. V. Sargsyan, and W. Scheid, *Phys. Rev. C* **81**, 057602 (2010).
 [16] L. Zhu, J. Su, and P. W. Wen, *Phys. Rev. C* **95**, 044608 (2017).
 [17] L. Zhu, P. W. Wen, C. J. Lin, X. J. Bao, J. Su, C. Li, and C. C. Guo, *Phys. Rev. C* **97**, 044614 (2018).
 [18] L. Zhu, J. Su, W. J. Xie, and F. S. Zhang, *Phys. Lett. B* **767**, 437 (2017).
 [19] X. J. Bao, S. Q. Guo, H. F. Zhang, and J. Q. Li, *Phys. Rev. C* **97**, 024617 (2018).
 [20] X. J. Bao, S. Q. Guo, H. F. Zhang, and J. Q. Li, *Phys. Lett. B* **785**, 221 (2018).
 [21] S. Q. Guo, X. J. Bao, H. F. Zhang, J. Q. Li, and N. Wang, *Phys. Rev. C* **100**, 054616 (2019).
 [22] Z. Q. Feng, *Phys. Rev. C* **95**, 024615 (2017).
 [23] P. H. Chen, F. Niu, W. Zuo, and Z. Q. Feng, *Phys. Rev. C* **101**, 024610 (2020).
 [24] A. V. Karpov and V. V. Saiko, *Phys. Rev. C* **96**, 024618 (2017).
 [25] P. W. Wen, A. K. Nasirov, C. J. Lin, and H. M. Jia, *J. Phys. G: Nucl. Part. Phys.* **47**, 075106 (2020).
 [26] X. J. Bao, *Phys. Rev. C* **102**, 054613 (2020); **102**, 064604 (2020); **104**, 034604 (2021).
 [27] Z. Cheng and X. J. Bao, *Phys. Rev. C* **103**, 024613 (2021).
 [28] Z. Cheng and X. J. Bao, *Phys. Rev. C* **103**, 064613 (2021).
 [29] X. J. Bao, S. Q. Guo, and P. H. Chen, *Phys. Rev. C* **105**, 024610 (2022).
 [30] A. Winther, *Nucl. Phys. A* **572**, 191 (1994).
 [31] A. Winther, *Nucl. Phys. A* **594**, 203 (1995).
 [32] R. Yanez and W. Loveland, *Phys. Rev. C* **91**, 044608 (2015).
 [33] V. Zagrebaev and W. Greiner, *Phys. Rev. Lett.* **101**, 122701 (2008).
 [34] V. I. Zagrebaev and W. Greiner, *Phys. Rev. C* **83**, 044618 (2011).
 [35] V. I. Zagrebaev and W. Greiner, *Phys. Rev. C* **87**, 034608 (2013).
 [36] K. Sekizawa and K. Yabana, *Phys. Rev. C* **88**, 014614 (2013).
 [37] K. Sekizawa, *Phys. Rev. C* **96**, 041601(R) (2017).
 [38] K. Godbey, C. Simenel, and A. S. Umar, *Phys. Rev. C* **101**, 034602 (2020).
 [39] X. Jiang and N. Wang, *Phys. Rev. C* **101**, 014604 (2020).
 [40] Z. J. Wu and L. Guo, *Phys. Rev. C* **100**, 014612 (2019).
 [41] X. Jiang and N. Wang, *Front. Phys.* **8**, 38 (2020).

- [42] S. Ayik, B. Yilmaz, O. Yilmaz, A. S. Umar, and G. Turan, *Phys. Rev. C* **96**, 024611 (2017).
- [43] S. Ayik, B. Yilmaz, O. Yilmaz, and A. S. Umar, *Phys. Rev. C* **97**, 054618 (2018).
- [44] C. Li, C. A. T. Sokhna, X. Xu, J. Li, G. Zhang, B. Li, Z. Ge, and F. S. Zhang, *Phys. Rev. C* **99**, 034619 (2019).
- [45] G. J. Li and X. J. Bao, *Phys. Rev. C* **107**, 024611 (2023).
- [46] T. L. Zhao, X. J. Bao, and H. F. Zhang, *Chin. Phys. C* **45**, 074108 (2021).
- [47] G. G. Adamian *et al.*, *Int. J. Mod. Phys. E* **05**, 191 (1996).
- [48] Q. Li, W. Zuo, W. Li *et al.*, *Eur. Phys. J. A* **24**, 223 (2005).
- [49] C. Y. Wong, *Phys. Rev. Lett.* **31**, 766 (1973).
- [50] R. J. Charity, *Phys. Rev. C* **82**, 014610 (2010).
- [51] D. Mancusi, R. J. Charity, and J. Cugnon, *Phys. Rev. C* **82**, 044610 (2010).
- [52] T. L. Zhao, X. J. Bao, and H. F. Zhang, *J. Phys. G: Nucl. Part. Phys.* **50**, 045101 (2023).
- [53] V. E. Viola and T. Sikkeland, *Phys. Rev.* **128**, 767 (1962).
- [54] K. Sandhu, M. K. Sharma, A. Kaur, and R. K. Gupta, *Phys. Rev. C* **90**, 034610 (2014).
- [55] T. L. Zhao, X. J. Bao, and H. F. Zhang, *Nucl. Phys. A* **1027**, 122510 (2022).
- [56] Y. A. Lazarev, Y. V. Lobanov, Y. T. Oganessian, V. K. Utyonkov, F. S. Abdullin, A. N. Polyakov, J. Rigol, I. V. Shirokovsky, Y. S. Tsyganov, S. Iliev, V. G. Subbotin, A. M. Sukhov, G. V. Buklanov, A. N. Mezentsev, K. Subotic, K. J. Moody, N. J. Stoyer, J. F. Wild, and R. W. Loughheed, *Phys. Rev. C* **62**, 064307 (2000).
- [57] V. Zagrebaev and W. Greiner, *Phys. Rev. C* **78**, 034610 (2008).